Dynamics of Charge Separation and Trap-Limited Electron Transport in TiO_2 Nanostructures

Juan A. Anta,*,† Iván Mora-Seró,‡ Thomas Dittrich,§ and Juan Bisquert‡

Departamento de Sistemas Físicos, Químicos y Naturales, Universidad Pablo de Olavide, 41013 Sevilla, Spain, Departament de Física, Universitat Jaume I, 12071 Castello, Spain, and Hahn-Meitner-Institut, Glienicker Strasse 100, D-14109 Berlin, Germany

Received: May 16, 2007; In Final Form: June 21, 2007

The dynamics of charge separation and transport in metal-oxide nanostructures used in nanocomposite solar cells is measured by time-resolved surface photovoltage (SPV) and described by random walk numerical simulations (RWNS). Characteristic features of anomalous diffusion and trap-limited electron transport are observed in SPV transients measured on a porous TiO_2 layer sensitized with N3 dye molecules. RWNS carried out on a three-dimensional cubic lattice with an exponential distribution of states can describe these transients quantitatively over many orders of magnitude in time. The RWNS reproduce the main experimental features and permit us to extract the microscopic parameters governing electron transport such as the characteristic trap energy and the screening length.

Charge separation and transport on the nanometer scale play an important role in many systems such as potentially low-cost photovoltaic devices based on nanocomposites. In nanocomposite solar cells two materials with different electrical behavior form interpenetrated networks for separate transport of positive and negative charge. Besides dye-sensitized solar cells (DSC)[1] organic polymer solar cells and solar cells with extremely thin absorber belong to the nanocomposite solar cells. A key process in the functioning of such devices is the transport of electrons through the network of interconnected nanoparticles or molecules. Anomalous or dispersive transport[2] features are normally observed in nanocomposites, that is, extremely slow transport combined with light intensity-dependent diffusion coefficients[3] and power law instead of exponential decays.[4] Multiple trapping (MT) diffusion of electrons injected into TiO_2 (in DSC) is the most prominent example.[5] In this article we apply a random walk numerical simulation (RWNS) that can deal efficiently with these anomalous features as observed in transient photovoltage measurements. We show that the combination of surface photovoltage (SPV) measurements and RWNS calculations provides a very direct way to probe the trap energy distribution and gives access to the main parameters influencing charge separation and transport.

There has been great interest in describing the trap-limited electron transport in nanoporous TiO_2.[6] Nelson and co-workers[4,7,8] applied a continuous time random walk (CTRW) simulation method (on which the numerical method applied in the present work is based) to describe transient absorption experiments. Van de Lagemaat and co-workers also applied numerical simulation random walk methods to describe transient photocurrent experiments.[9,10] Several authors have used charging−discharging methods to determine the distribution of traps: cyclic voltammetry,[11] capacitance spectroscopy,[12] voltage-decay charge-extraction method,[13,14] and potential step-current integration (chronoamperometry).[15,16] Peter and co-workers first found the Fermi-level dependence of electron diffusion coefficients[3] and recently reviewed the characteristics of trap distributions and electron transport in DSC,[17] including the explanation of observed activation energies[18] and direct measurement of the Fermi level.[19] Bisquert and co-workers have described the trap-limited transport theoretically, using the quasi-static approximation,[20,21] and experimentally, using impedance spectroscopy.[5,12]

These contributions and others have provided a consistent view of electron transport in nanostructured TiO_2 and DSC that is basically coherent with an MT model with an exponential distribution of states in the band gap. However, most of the experimental methods only probe the external contacts (i.e., charge collected or Fermi level) or an integration over the whole film in optical absorption measurements. Such type of evidence is indirect to a certain extent as it does not address the electron dynamics *inside* the nanostructure. Important questions concerning how the traps influence transient measurements on DSCs are still not unambiguously known.

In recent work, we have presented a series of studies of electron dynamics in nanoporous and ultrathin TiO_2 layers by SPV transients.[22−24] With respect to the other aforementioned experimental methods, SPV has the advantage that it detects the advancement of electrons diffusing in TiO_2 with spatial and dynamic resolution on very short scales. In this article we aim to model SPV transients in porous TiO_2 layers under identical conditions as described recently.[23] The layers were prepared on SnO_2:F substrates by screen printing of a paste containing anatase nanoparticles (16 nm diameter) and by subsequent firing in air at 450 °C for 30 min. The samples were sensitized by dipping in 0.5 M N3 ($Ru(dcbpyH_2)_2(NCS)_2$) dye solution for 10 s. The low exposition time of the sample to the dye solution ensures that only the surface region of the porous samples was sensitized. The transients were measured with a repetition rate of 1 Hz.

This experimental configuration is schematically described in Figure 1a; electrons injected from N3 dye molecules attached at the outer edge of a nanostructured TiO_2 layer diffuse into

† Universidad Pablo de Olavide.
‡ Universitat Jaume I.
§ Hahn-Meitner-Institut.

10.1021/jp0737909 CCC: $37.00
Published on Web 08/28/2007

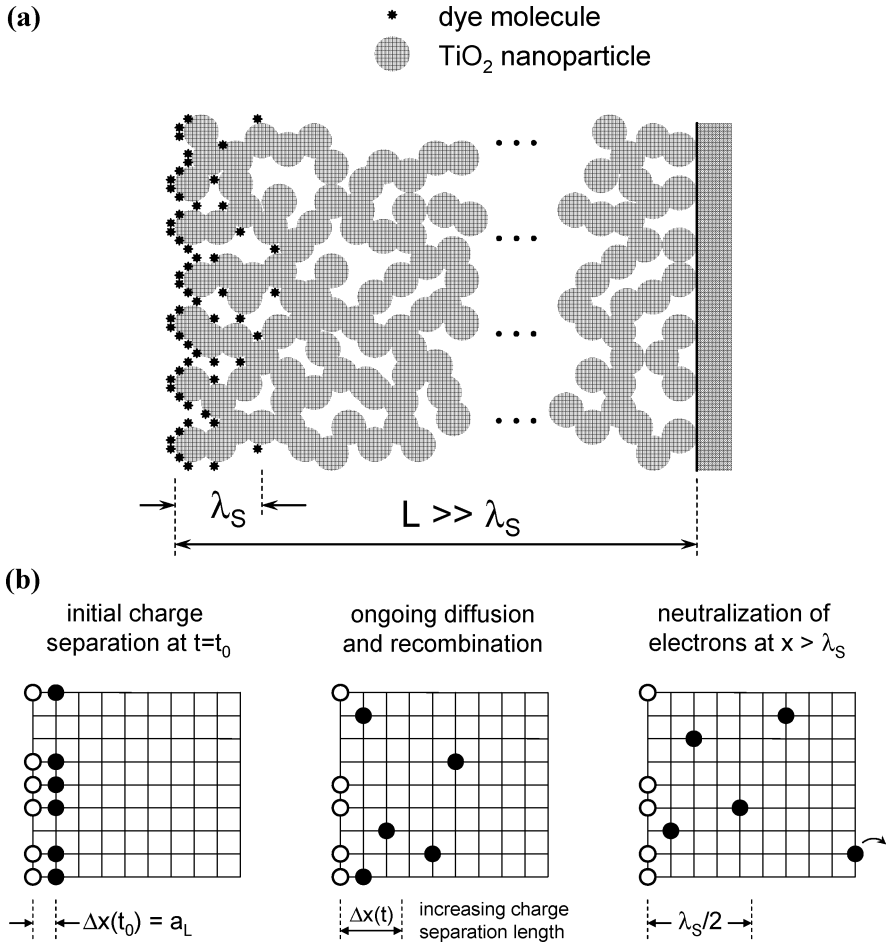

Figure 1. (a) Sketch of the investigated structure consisting of an interconnected network of TiO_2 nanoparticles dyed in the outer surface region. The screening length of the system (λ_S) is much shorter than the sample thickness (taken from ref 23). (b) Scheme of elementary processes considered in the model (projection into $x-y$ plane, RWNS on a 3D cubic lattice). The surface photovoltage (SPV) is given by the amount of separated charge and by the effective charge separation length. The positive charge (open circles) is fixed at the surface, whereas electrons (filled circles) are mobile. The electrons move between neighbored traps that are distributed in an ideal cubic lattice (lattice constant a_L). Moves are forbidden to occupied neighbored sites.

the layer. The measured SPV consists on the voltage due to the separation between the negative (electrons) and positive (oxidized N3 dyes) charge.[25] The sample is measured in vacuum conditions, and the charge separation is detected on capacitor configuration.[23] The transient SPV is recorded over 8 decades in time from nanoseconds to 0.1 s and displays a broad peak. The rising part of the peak is interpreted as an increase of the distance of charge separation, while the decaying part is ascribed to the fact that those electrons that reach the screening length (λ_S) do not further contribute to measured SPV.[23] An important aspect of these results is that the shorter time parts of the transients clearly display a power law dependence of time

$$V(t) \propto t^{\alpha/2} \tag{1}$$

Equation 1 follows from the mean square displacement for the anomalous diffusion model ($r^2 \propto C_\alpha t^\alpha$).[26] With the use of these concepts, an heuristical description of the experimental results has been presented in previous work.[23,24] However, it is characteristically difficult to solve analytical models with energy disorder in spatially inhomogeneous situations. This has prevented a quantitative description of the transients, which is important in order to extract the parameters such as the characteristic trap energy and the screening length.

The RWNS method is a stochastic calculation that permits us to obtain transient currents and electron lifetimes,[4,8,9] as well as steady-state electron mobilities[8] without huge computational demands. In previous work[24] we applied the RWNS method to model SPV transients in compact, ultrathin TiO_2 films. Here we extend these calculations to the description of the SPV transients in mesoporous TiO_2. The main result is that the simulations are able to accurately describe the transients over a broad range of time decades and provide access to the microscopic parameters that govern the electrons dynamics. More concretely, we investigate the dynamics of charge separation by RWNS on a three-dimensional (3D) cubic lattice of trap sites with the lattice constant a_L. A two-dimensional illustration of the RWNS method employed is shown in Figure 1b. The positive charge is fixed at the surface, whereas electrons are mobile. The electrons move between neighbored traps that are distributed in an ideal cubic lattice. A move is forbidden if the neighbored trap is already occupied. The charge separation, i.e., the separation of centers of positive and negative charges,[25] is described in terms of time-dependent SPV which follows from the integration of the charge distribution via the Poisson equation.[22,25] Electrons reaching the screening length (λ_S) are removed from the sample since the screened or neutralized charge does not contribute any more to the SPV signal.[23] Periodic boundary conditions are applied along the directions parallel to the injecting plane (y and z). During the simulation the electrons adopt the *release times* of the sites that they visit. Each trap i with energy E_i (defined as the energy separation of

the trap with respect to the electron transport level) is given a release time, t_i, according to

$$t_i = -\frac{\ln(r)}{f} e^{E_i/kT} \quad (2)$$

where r is a random number uniformly distributed between 0 and 1, f is the so-called attempt-to-jump frequency, and T is the absolute temperature. The *waiting time* is the difference between the release time of an electron and the time already spent by that electron in its trap. For each simulation step the electron with the shortest waiting time (t_{min}) is moved to an empty neighbored site chosen at random. This time is then used to advance the total simulation time and to reduce accordingly the waiting times of the rest of the electrons. Hence, the simulation is advanced by time increments that depend on the traps occupied at the current simulation time. This is crucial to reproduce experimental phenomena that take place over many decades in time.

The trap energies are distributed exponentially as follows:

$$g(E) = \frac{N_t}{k_B T_0} \exp\left(\frac{E}{k_B T_0}\right) \quad (3)$$

where N_t is the total trap density, k_B is the Boltzmann's constant, and T_0 is the distribution parameter in temperature units. Power law coefficients in the MT model (eq 1) are related to the parameter of the trap distribution via the relationship $\alpha = T/T_0$.[27] In TiO_2 layers, values of T_0 range usually between 500[28] and 900 K[29] depending on preparation and measurement conditions. Characteristic values of the total trap density are in the range of $N_t = 10^{20}-10^{21}$ cm^{-3} for porous TiO_2[11] implementing a mean distance between neighbored traps of about 1−3 nm.

The previous formalism represents the diffusive displacement of electrons in the traps distribution, whereas the SPV is calculated by integrating the negative charge density. The possible influence of the electrical field induced by the charge on transport has been explored in additional simulations (not shown). It was observed that fields much larger than those created by the small electron densities used here are required in order to modify the diffusion results.

Before describing the experimental data, we discuss some simulation results that illustrate the main characteristics of the model. Figure 2 shows simulated SPV transients at $T = 300$ K for a distribution $T_0 = 700$ K with different lattice constants and screening lengths. All simulated SPV transients increase in time, reach their maximum at t_{peak}, and decay at longer times. As expected from the increasing number of sites in the x-direction, the values of t_{peak} increase with decreasing a_L or increasing λ_S. The shapes of the SPV transients in the log−log plots are practically independent of the values of a_L or λ_S (there is only some change at very short time for the smallest a_L). Although not shown, it is observed that t_{peak} follows a power law with power coefficients of $-2/\alpha$ and $2/\alpha$ for the dependencies of t_{peak} on a_L and λ_S, respectively. This indicates the equivalence of both parameters with respect to an average number of jumping events until all electrons run out of the box. Therefore, the parameter a_L will be fixed at 2 nm hereafter.

The combination of RWNS and SPV measurements permit us to estimate the value of T_0, the most important parameter in the MT theory with exponential distribution of trap energies. The SPV transients depicted in Figure 3 were simulated for identical values of a_L and λ_S, whereas T_0 was varied between 300 and 900 K. It should be remarked that a variation of $1/T$ will give analogous results. The shapes of the SPV transients

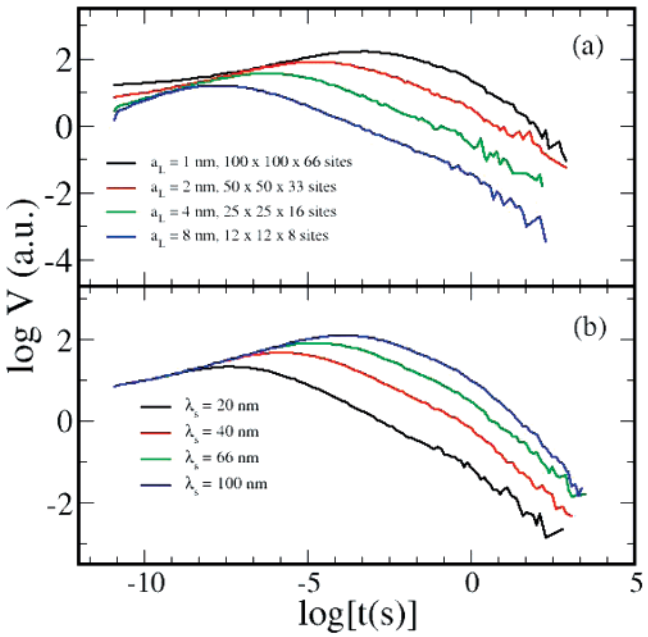

Figure 2. Surface photovoltage (SPV) transients simulated for different lattice constants (a) and different screening lengths (b). The simulations for $T_0 = 700$ and $T = 300$ K. The value of λ_S was set to 66 nm (a), whereas the value of a_L was set 2 nm (b).

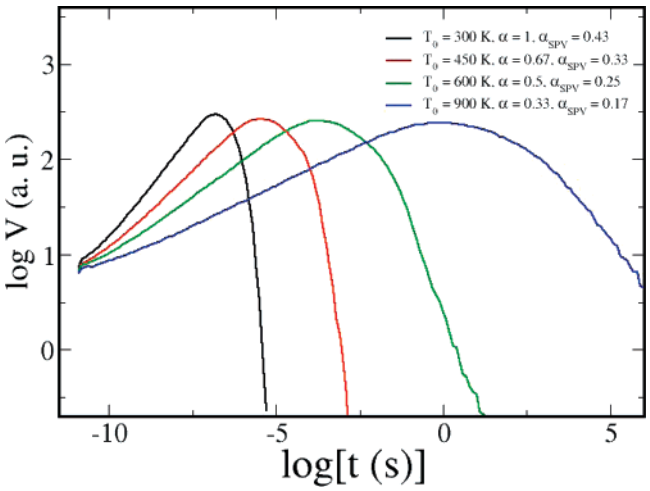

Figure 3. Surface photovoltage (SPV) transients simulated for different characteristic temperatures ($a_L = 2$ nm, $\lambda_S = 200$ nm, and $T = 300$ K). The correlation between α (α = T/T_0) and the fitted power coefficient of the SPV at shorter times α_{SPV} is shown in the legend.

depend dramatically on T_0. For example, t_{peak} varies over more than 6 orders of magnitude for the given range of T_0. It should be noticed that the modeled SPV transients present a power law dependence on time at the shorter times.

Figure 4 depicts measured and simulated SPV transients. We used the following procedure to get T_0 and λ_S: the values of a_L, and f, were fixed at 2 nm and 10^{11} Hz, respectively. These assumptions make sense with respect to previous experimental findings provided the intensities of the laser pulses for excitation are not very high. The value of T_0 served as a fit parameter for the SPV transients at shorter times. Then, the value of t_{peak} can be well fitted by choosing λ_S. The values of T_0 increase from about 550 K at 150 K to about 800 K at 400 K and remain constant at higher temperatures. These values are consistent with the exponential distributions normally employed in the literature to describe transport in porous TiO_2 films.[3,8,12] Variations in

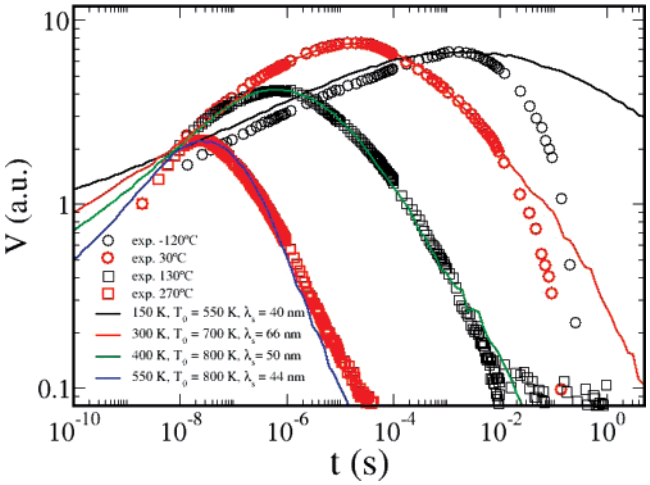

Figure 4. Experimentally obtained surface photovoltage (SPV) transients (symbols) of dyed nanoporous TiO_2 measured at different temperatures and simulated SPV transients (lines) with best coincidence. The repetition rate of the Nd:YAG laser pulses was 1 Hz and leads to some stationary charging at the lower temperatures (not considered in the RWNS simulations). The RWNS simulations were performed for $a_L = 2$ nm and $F = 0$ V/cm. The values of T_0 and λ_S utilized in the fittings are indicated in the legend.

trap distribution with temperature have also been observed in other works.[30]

On another hand, the SPV transients are very well described over the whole time range by our RWNS method at the higher temperatures if values for λ_S of 50 nm at 400 K and 44 nm at 550 K are assumed. For these temperatures the SPV transients are much shorter than the inverse repetition rate of the laser pulses. We remark that the screening lengths obtained by our procedure from measured SPV transients with RWNS are of the same order as the screening lengths calculated from time-of-flight measurements under electron injection condition.[31]

At lower temperatures, it is not possible to fit the measured SPV transients for times longer than 10^{-2} s. The RC time constant of the capacitor and the measurement resistance is about 0.3 s, i.e., the SPV transients can be measured well only at shorter times. For the given temperatures the simulated SPV transients exceed strongly 1 s. Therefore, the conditions of the RWNS differ significantly from the experimental conditions since a repetition rate of laser pulses of 1 Hz was used. This means that some permanent charging of the deepest traps takes place in the experiments at lower temperatures.

In previous work[24] we showed that the RWNS was reproducing the general trends observed in SPV of compact ultrathin films. In the present work, we have demonstrated for the first time quantitative agreement of simulation and experimental results. This is strong evidence that electron trapping is governing the dynamics of the injected charge. In addition, in contrast to our previous simulations results for compact films, in the present RWNS calculations electrons are removed in the simulation only when they reach the screening length, without recombination terms. This model successfully reproduces the transients of porous TiO_2 samples while keeping a low number of fitting parameters. Electron removal by recombination is required to model SPV transients in ultrathin TiO_2 films, where the photovoltage decays are mainly controlled by recombination to dye molecules adsorbed to the surface.[22]

In conclusion, the dynamics of charge separation measured by SPV transients in characteristic TiO_2 nanostructures used in DSCs are well described over many orders of magnitude in time by RWNS method in a lattice of traps. Therefore, RWNS is an ideal tool for the quantitative description of experimental SPV transients[24] and hence for empirically determining parameters governing anomalous charge transport which are rather difficult to obtain through alternative experimental techniques. Parameters which can be obtained are the characteristic temperature of the exponential trap distribution, the screening length, the trap density, and the attempt-to-jump frequency. The RWNS method is computationally simple and versatile and opens the way to study more sophisticated trap distributions, geometries different from cubic lattices, influence of recombination mechanisms, etc., all of them not easily accessible to methods based on continuity equations.

Acknowledgment. The work was supported by Ministerio de Educación y Ciencia of Spain under projects MAT2004-05168 and ENE2004-01657/ALT.

References and Notes

(1) O'Regan, B.; Grätzel, M. *Nature* **1991**, *353*, 737.
(2) Scher, H.; Montroll, E. W. *Phys. Rev. B* **1975**, *12*, 2455.
(3) Fisher, A. C.; Peter, L. M.; Ponomarev, E. A.; Walker, A. B.; Wijayantha, K. G. U. *J. Phys. Chem. B* **2000**, *104*, 949.
(4) Nelson, J. *Phys. Rev. B* **1999**, *59*, 15374.
(5) Wang, Q.; Ito, S.; Grätzel, M.; Fabregat-Santiago, F.; Mora-Seró, I.; Bisquert, J.; Bosshoa, T.; Imaic, H. *J. Phys. Chem. B* **2006**, *110*, 19406.
(6) de Jongh, P. E.; Vanmaekelbergh, D. *Phys. Rev. Lett.* **1996**, *77*, 3427.
(7) Nelson, J.; Haque, S. A.; Klug, D. R.; Durrant, J. R. *Phys. Rev. B* **2001**, *63*, 205321.
(8) Anta, J. A.; Nelson, J.; Quirke, N. *Phys. Rev. B* **2002**, *65*, 125324.
(9) van de Lagemaat, J.; Frank, A. J. *J. Phys. Chem. B* **2001**, *105*, 11194.
(10) van de Lagemaat, J.; Kopidakis, N.; Neale, N. R.; Frank, A. J. *Phys. Rev. B* **2005**, *71*, 035304.
(11) Fabregat-Santiago, F.; Mora-Seró, I.; Garcia-Belmonte, G.; Bisquert, J. *J. Phys. Chem. B* **2003**, *107*, 758.
(12) Fabregat-Santiago, F.; Bisquert, J.; Garcia-Belmonte, G.; Boschloo, G.; Hagfeldt, A. *Sol. Energy Mater. Sol. Cells* **2005**, *87*, 117.
(13) Peter, L. M.; Duffy, N. W.; Wang, R. L.; Wijayantha, K. G. U. *J. Electroanal. Chem.* **2002**, *524*−*525*, 127.
(14) Boschloo, G.; Hagfeldt, A. *J. Phys. Chem. B* **2005**, *109*, 12093.
(15) Palomares, E.; Clifford, J. N.; Haque, S. A.; Lutz, T.; Durrant, J. R. *J. Am. Chem. Soc.* **2003**, *125*, 475.
(16) Agrell, H. G.; Boschloo, G.; Hagfeldt, A. *J. Phys. Chem. B* **2004**, *108*, 12388.
(17) Peter, L. M. *J. Phys. Chem. C* **2007**, *111*, 6601.
(18) Peter, L. M.; Walker, A. B.; Boschloo, G.; Hagfeldt, A. *J. Phys. Chem. B* **2006**, *110*, 13694.
(19) Lobato, K.; Peter, L. M. *J. Phys. Chem. B* **2006**, *110*, 21920.
(20) Bisquert, J. *J. Phys. Chem. B* **2004**, *108*, 2323.
(21) Bisquert, J.; Vikhrenko, V. S. *J. Phys. Chem. B* **2004**, *108*, 2313.
(22) Mora-Seró, I.; Dittrich, T.; Belaidi, A.; Garcia-Belmonte, G.; Bisquert, J. *J. Phys. Chem. B* **2005**, *109*, 14932.
(23) Dittrich, T.; Mora-Seró, I.; Garcia-Belmonte, G.; Bisquert, J. *Phys. Rev. B* **2006**, *73*, 045407.
(24) Mora-Seró, I.; Anta, J. A.; Garcia-Belmonte, G.; Dittrich, T.; Bisquert, J. *J. Photochem. Photobiol., A* **2006**, *182*, 280−287.
(25) Mora-Seró, I.; Dittrich, T.; Garcia-Belmonte, G.; Bisquert, J. *J. Appl. Phys.* **2006**, *100*, 103705.
(26) Metzler, R.; Barkai, E.; Klafter, J. *Phys. Rev. Lett.* **1999**, *82*, 3563.
(27) Orenstein, J.; Kastner, M. *Phys. Rev. Lett.* **1981**, *46*, 1421.
(28) Duzhko, V.; Timoshenko, V. Y.; Koch, F.; Dittrich, T. *Phys. Rev. B* **2001**, *64*, 075204.
(29) Dittrich, T.; Zinchuk, V.; Skryshevskyy, V.; Urban, I.; Hilt, O. *J. Appl. Phys.* **2005**, *98*, 104501.
(30) Abayev, I.; Zaban, A.; Kytin, V. G.; Danilin, A. A.; Garcia-Belmonte, G.; Bisquert, J. *J. Solid State Electrochem.* **2007**, *11*, 647−653.
(31) Kytin, V.; Dittrich, T.; Bisquert, J.; Lebedev, E. A.; Koch, F. *Phys. Rev. B* **2003**, *68*, 195308.